Asia Pac. J. Math. 2026 **13**:45

MHD IMPACT ON PERISTALTIC TRANSPORT OF A PSEUDOPLASTIC NANOFLUID THROUGH POROUS MEDIUM IN INCLINED ASYMMETRIC CHANNEL

M. H. ALI*, M. R. SALMAN

Department of Mathematics, College of Education for Pure Sciences, University of Karbala, Karbala, Iraq

*Corresponding author: mahmood.ali@s.uokerbala.edu.iq

Received Feb. 9, 2026

Abstract. This research is dedicated to study the peristaltic transport of a pseudoplastic nano-fluid with inclined asymmetric channel incorporating a porous medium under magnetohydrodynamic (MHD) effects with convective conditions of the boundary applied on the channel walls. Shape of the wall was represented using a periodic harmonic wave based on a sine function, reflecting the oscillatory nature of peristaltic motion. A mathematical model was developed that included momentum, continuity, and energy equations, assuming a large wavelength and a small Reynolds number. Equations were solved by perturbation method to get approximate solutions, and then numerically using MATHEMATICA 14. The results were then analyzed graphically by physical parameters (for example the Hartmann number, thermophoresis coefficient in addition to permeability coefficient) affecting the temperature profile, velocity profile, heat transfer coefficient as well as pressure rise. The analysis also included the phenomena of trapping and pumping, which are characteristic features of peristaltic flow in such channels.

2020 Mathematics Subject Classification. 76W05, 76S05, 76U05.

Key words and phrases. peristaltic transport; magnetohydrodynamic; stream function; Reynolds number.

1. Introduction

Peristaltic transport is a fundamental fluid motion mechanism, induced through periodic deformations of the transport channel, pushing the fluid in a specific direction without the need for external pressure. This mechanism has an important role in biological systems, For example, the movement of ingested materials, the passage of food through the digestive system and the flow of urine from the kidneys system to the bladder as well as the flow of bile through its ducts.

Our model's incorporation of MHD, porous medium, and inclined channel effects mirrors actual physical circumstances in geophysical, industrial, and medical applications where these effects coexist. For instance, the following can be combined in micro medical devices like peristaltic micropumps, which use peristalsis to move non-Newtonian fluids like blood or polymer solutions.

DOI: 10.28924/APJM/13-45

Mathematically, modified Navier–Stokes flow equations allow for the inclusion of magnetic field (Lorentz force), porosity (Darcy/Forchheimer terms), and slope (gravitational component along the slope). Several published studies have addressed the integration of some of these factors with pseudoplastic nanofluid, thus justifying their inclusion in our research from both a physical and mathematical perspective. Our aim is to study the combined effect of these conditions on peristalsis, thereby filling an existing research gap and providing a scientific basis for various practical applications.

The first studies on the phenomenon of peristalsis began with the researcher [12] early contributions marked an important starting point in understanding the mechanisms of undulation pumping, as he investigated pump performance, internal flow patterns, and mixing resulting from secondary motions. These findings became the cornerstone of subsequent developments in the study of undulation, then it became of interest to many researchers (see studies [1,4,7–9,11,14,16–18]). The field of nanofluids has witnessed increasing interest in recent years, driven by its diverse biological and engineering applications, particularly in the fields of biochemistry, medicine, and advanced technologies. For the first time [3] introduced the term nano-fluid to describe a fluid containing nanoparticles with diameters typically below 50 nanometers. These particles may be composed of metallic substances such as aluminum, copper, aluminum oxide, silicon nitride, and silicon carbide, or non-metallic materials including carbon, graphite, carbon nanotubes, nanosheets, nanofibers, and nanodroplets.

Current interest focuses on examining how magnetohydrodynamics affects pseudoplastic nanofluid peristaltic transport in an asymmetric channel, which is characterised by flexible walls.

It is known that the viscosity or apparent consistency of these fluids decreases rapidly with increasing shear rate [5]. Asymmetric wall vibrations have also been observed in some biological channels. Eytan et al. in 1999 and Ali & Salman, in 2024 studied the effect of rotation of non-Newtonian fluids inside a corrugated channel [2,6]. A comparative investigation was conducted into the peristaltic transport of nanofluids suspended in aqueous media [19]. Tripathi & Bég, in 2014, investigating how nanofluid characteristics affect peristaltic transport [20]. Hina et al., in 2015, conducted a comprehensive study on the peristaltic movement of pseudoplastic fluid in a channel curving [10], taking into account all relevant physical characteristics as well as the impact of thermal and mass transfer. Researchers are interested in this crucial area because stones in the ureters and bile ducts serve as models for porous media in channels [13,15]. The purpose of this work is to examine the peristaltic motion of a pseudoplastic nanofluid in an asymmetric channel with a porous medium when an external magnetic field is present. The oscillatory nature of peristaltic motion is reflected in the wall shape, which is described by a periodic harmonic wave based on a sine function. The perturbation method is used to obtain approximate solutions for the momentum, continuity, and energy equations under the assumption of a large wavelength and a small number of Reynolds. Mathematica software is then used

to graphically analyse how various factors affect temperature, velocity profile, heat transfer coefficient, and pressure rise. Pumping and trapping phenomena are also investigated.

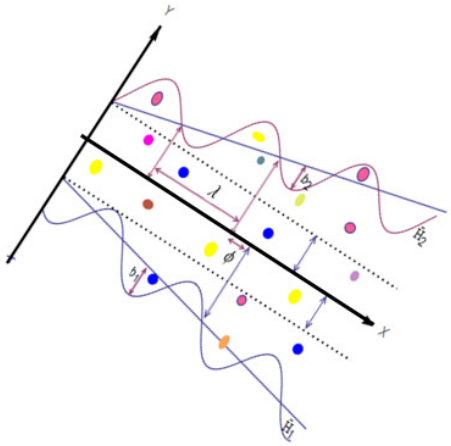

FIGURE 1. Geometry of an asymmetric channel.

2. PROBLEM FORMULATION

This work examines the magnetohydrodynamic peristaltic motion of an incompressible pseudoplastic nanofluid influence (MHD) effects in inclined asymmetric channel in two dimensions width 2d and filled with porous medium. Peristaltic waves propagate along $\bar{\varkappa}$-axix at velocity c, while Υ-axis is perpendicular to it [see Figure 1] where Υ_1 is the lower wall and Υ_2 is the upper wall. A homogeneous magnetic field $B = (0, B_0, 0)$ is apply in $\bar{\Upsilon}$-direction. The induced magnetic field can be disregarded because the magnetic Reynolds number is low. The electric field is also considered absent. Sinusoidal waves that travel along the elastic walls of the channel cause flow to develop. The wall surface geometry is specified as follows:

$$\bar{\Upsilon}_1 = \widetilde{H}_1 = -d - \acute{m}\bar{\varkappa} - b_1 \sin\left[\frac{2\pi}{\lambda}\left(\bar{\varkappa} - c\acute{t}\right) + \phi\right] \tag{1}$$

$$\bar{\Upsilon}_2 = \widetilde{H}_2 = d + \acute{m}\bar{\varkappa} + b_2 \sin\left[\frac{2\pi}{\lambda}\left(\bar{\varkappa} - c\acute{t}\right)\right] \tag{2}$$

Where the channel has a width of 2d and The asymmetric tapered channel's non-uniformity is represented by the parameter $(\acute{m} \ll 1)$. The amplitudes related to the upper and lower channel walls are denoted by b_1 and b_2, $\acute{t}$ is the dimensionless time, ϕ It describes the difference phase that varies between $0 \leq \phi \leq \pi$. Observe that we have an asymmetric channel with out-of-phase waves when $\phi = 0$. In addition, b_1, d, b_2 and ϕ satisfy the condition:

$$b_1^2 + b_2^2 + 2b_1 b_2 \cos(\phi) \leq (2d)^2 \tag{3}$$

In pseudoplastic fluids, the extra stress tensor is:

$$\breve{S}+\lambda_1\frac{D\breve{S}}{D\acute{t}}+\frac{1}{2}\left(\lambda_1-\mu_1\right)\left(I_1\breve{S}+\breve{S}I_1\right)=\mu I_1$$

Where λ_1 and μ_1 are relaxation times besides I_1 refers to Rivlin-Ericksen tensor. Also

$$I_1=\left[\nabla\vec{V}+\left(\nabla\vec{V}\right)^T\right],\ {}^{d\breve{S}}/_{d\acute{t}}={}^{\partial\breve{S}}/_{\partial\acute{t}}+\vec{V}.\nabla\breve{S},$$

$$\frac{D\breve{S}}{D\acute{t}}={}^{\partial\breve{S}}/_{\partial\acute{t}}+\vec{V}.\nabla\breve{S}-\left(\nabla\vec{V}\right)\breve{S}-\breve{S}\left(\nabla\vec{V}\right)^T.$$

The extra stress components $\breve{S}_{\bar{\varkappa}\bar{\varkappa}}, \breve{S}_{\bar{\varkappa}\bar{\Upsilon}}, \breve{S}_{\bar{\Upsilon}\bar{\varkappa}}$ and $\breve{S}_{\bar{\Upsilon}\bar{\Upsilon}}$ We can get it from the following relationships:

$$\begin{aligned}&\breve{S}_{\bar{\varkappa}\bar{\varkappa}}+\lambda_1\left[\left(\frac{\partial}{\partial\acute{t}}+\widetilde{U}\frac{\partial}{\partial\bar{\varkappa}}+\widetilde{V}\frac{\partial}{\partial\bar{\Upsilon}}\right)\breve{S}_{\bar{\varkappa}\bar{\varkappa}}-2\breve{S}_{\bar{\varkappa}\bar{\varkappa}}\frac{\partial\widetilde{U}}{\partial\bar{\varkappa}}2\breve{S}_{\bar{\varkappa}\bar{\Upsilon}}\frac{\partial\widetilde{U}}{\partial\bar{\Upsilon}}\right]\\&+\frac{1}{2}\left(\lambda_1-\mu_1\right)\left[4\breve{S}_{\bar{\varkappa}\bar{\varkappa}}\frac{\partial\widetilde{U}}{\partial\bar{\varkappa}}+2\breve{S}_{\bar{\varkappa}\bar{\Upsilon}}\left(\frac{\partial\widetilde{U}}{\partial\bar{\Upsilon}}+\frac{\partial\widetilde{V}}{\partial\bar{\varkappa}}\right)\right]=2\mu\frac{\partial\widetilde{U}}{\partial\bar{\varkappa}}\end{aligned}\tag{4}$$

$$\begin{aligned}&\breve{S}_{\bar{\varkappa}\bar{\Upsilon}}+\lambda_1\left[\left(\frac{\partial}{\partial\acute{t}}+\widetilde{U}\frac{\partial}{\partial\bar{\varkappa}}+\widetilde{V}\frac{\partial}{\partial\bar{\Upsilon}}\right)\breve{S}_{\bar{\varkappa}\bar{\Upsilon}}-\breve{S}_{\bar{\varkappa}\,\bar{\varkappa}}\frac{\partial\widetilde{V}}{\partial\bar{\varkappa}}-\breve{S}_{\bar{\Upsilon}\bar{\Upsilon}}\frac{\partial\widetilde{U}}{\partial\bar{\Upsilon}}\right]\\&+\frac{1}{2}\left(\lambda_1-\mu_1\right)\left(\breve{S}_{\bar{\varkappa}\bar{\varkappa}}+\breve{S}_{\bar{\Upsilon}\bar{\Upsilon}}\right)\left(\frac{\partial\widetilde{U}}{\partial\bar{\Upsilon}}+\frac{\partial\widetilde{V}}{\partial\bar{\varkappa}}\right)=\mu\left(\frac{\partial\widetilde{U}}{\partial\bar{\Upsilon}}+\frac{\partial\widetilde{V}}{\partial\bar{\varkappa}}\right)\end{aligned}\tag{5}$$

$$\begin{aligned}&\breve{S}_{\bar{\Upsilon}\bar{\Upsilon}}+\lambda_1\left[\left(\frac{\partial}{\partial\acute{t}}+\widetilde{U}\frac{\partial}{\partial\bar{\varkappa}}+\widetilde{V}\frac{\partial}{\partial\bar{\Upsilon}}\right)\breve{S}_{\bar{\Upsilon}\bar{\Upsilon}}-2\breve{S}_{\bar{\Upsilon}\bar{\varkappa}}\frac{\partial\widetilde{V}}{\partial\bar{\varkappa}}-2\breve{S}_{\bar{\Upsilon}\bar{\Upsilon}}\frac{\partial\widetilde{V}}{\partial\bar{\Upsilon}}\right]\\&+\frac{1}{2}\left(\lambda_1-\mu_1\right)\left[2\breve{S}_{\bar{\varkappa}\bar{\Upsilon}}\left(\frac{\partial\widetilde{U}}{\partial\bar{\Upsilon}}+\frac{\partial\widetilde{V}}{\partial\bar{\varkappa}}\right)+4\breve{S}_{\bar{\Upsilon}\bar{\Upsilon}}\frac{\partial\widetilde{V}}{\partial\bar{\Upsilon}}\right]=2\mu\frac{\partial\widetilde{V}}{\partial\bar{\Upsilon}}\end{aligned}\tag{6}$$

3. Method of Solution

The equation of continuity can be expressed as:

$$\frac{\partial\widetilde{U}}{\partial\bar{\varkappa}}+\frac{\partial\widetilde{V}}{\partial\bar{\Upsilon}}=0\tag{7}$$

The momentum equations:

$$\rho_f\left[\frac{\partial\widetilde{U}}{\partial\acute{t}}+\widetilde{U}\frac{\partial\widetilde{U}}{\partial\bar{\varkappa}}+\widetilde{V}\frac{\partial\widetilde{U}}{\partial\,\bar{\Upsilon}}\right]=-\frac{\partial\widetilde{P}}{\partial\bar{\varkappa}}+\frac{\partial}{\partial\bar{\varkappa}}\left(\breve{S}_{\bar{\varkappa}\bar{\varkappa}}\right)+\frac{\partial}{\partial\,\bar{\Upsilon}}\left(\breve{S}_{\bar{\varkappa}\,\bar{\Upsilon}}\right)-\acute{o}B_0^2\widetilde{U}-\frac{\mu}{K_0}\widetilde{U}+\rho_f g\sin\alpha\tag{8}$$

$$\rho_f\left[\frac{\partial\widetilde{V}}{\partial\acute{t}}+\widetilde{U}\frac{\partial\widetilde{V}}{\partial\bar{\varkappa}}+\widetilde{V}\frac{\partial\widetilde{V}}{\partial\bar{\Upsilon}}\right]=-\frac{\partial\widetilde{P}}{\partial\bar{\Upsilon}}+\frac{\partial}{\partial\bar{\varkappa}}\left(\breve{S}_{\bar{\Upsilon}\bar{\varkappa}}\right)+\frac{\partial}{\partial\bar{\Upsilon}}\left(\breve{S}_{\bar{\Upsilon}\bar{\Upsilon}}\right)-\frac{\mu}{K_0}\widetilde{V}-\rho_f g\cos\alpha\tag{9}$$

The governing equation for nanoparticle temperature:

$$\left(\rho\acute{c}\right)_f\left[\frac{\partial\widetilde{T}}{\partial\acute{t}}+\widetilde{U}\frac{\partial\widetilde{T}}{\partial\bar{\varkappa}}+\widetilde{V}\frac{\partial\widetilde{T}}{\partial\bar{\Upsilon}}\right]=\kappa\left[\frac{\partial^2\widetilde{T}}{\partial\bar{\varkappa}^2}+\frac{\partial^2\widetilde{T}}{\partial\bar{\Upsilon}^2}\right]+\left(\rho\acute{c}\right)_p\frac{D_T}{T_m}\left[\left(\frac{\partial\widetilde{T}}{\partial\bar{\varkappa}}\right)^2+\left(\frac{\partial\widetilde{T}}{\partial\bar{\Upsilon}}\right)^2\right]\tag{10}$$

Symbols $\widetilde{V}$ and $\widetilde{U}$ denotes the transverse and axial velocity components, respectively. Some symbols employed in the present analysis are defined in a dedicated table named NUMERICALTURE. The governing boundary constraints, which include the no-slip and convective thermal boundaries, can be written as:

$$U = 0, \widetilde{T} = T_0 \ \ at \ \ \bar{\Upsilon}_1 = \check{H}_1 \tag{11}$$

$$U = 0, \widetilde{T} = T_1 \ \ at \ \ \bar{\Upsilon}_2 = \check{H}_2 \tag{12}$$

To simplify variables, dimensionless quantities are defined as follows:

$$\left.\begin{array}{l} x = \dfrac{\varkappa}{\lambda}, y = \dfrac{\Upsilon}{d}, t = \dfrac{c\acute{t}}{\lambda}, u = \dfrac{\widetilde{u}}{c}, v = \dfrac{\widetilde{v}}{c}, \ \delta = \dfrac{d}{\lambda} \\ \grave{h}_2 = \dfrac{\widetilde{H}_2}{d}, \ \theta = \dfrac{\widetilde{T} - T_0}{T_1 - T_0} \ , \ p = \dfrac{d^2\widetilde{p}}{\lambda\mu c}, \ S_{ij} = \dfrac{d_1}{c\mu}\breve{S}_{\widetilde{ij}}, \lambda_1^* = \dfrac{\lambda_1 c}{d} \\ K = \dfrac{K_0}{d^2}, Re = \dfrac{\rho_f c d}{\mu}, a = \dfrac{b_1}{d}, b = \dfrac{b_2}{d}, m = \dfrac{\acute{m}\lambda}{d} \\ Nt = \dfrac{\tau D_T \left(T_1 - T_0\right)}{T_m \sqsubseteq}, M = \sqrt{\dfrac{\acute{\sigma}}{\mu}} dB_0, Fr = \dfrac{c^2}{gd}, u = \dfrac{\partial \Psi}{\partial y} \\ \grave{h_1} = \dfrac{\widetilde{H}_1}{d}, \mu_1^* = \dfrac{\mu_1 c}{d}, Pr = \dfrac{\mu \acute{c}_f}{\kappa}, v = -\delta \dfrac{\partial \Psi}{\partial x} \end{array}\right\} \tag{13}$$

Where the dimensionless parameters refer to the following quantities: y and x denote the axial and transverse coordinates, Fr the Froude number, Ψ the stream function.

A moving coordinate system (X, Y) with the same velocity c wave propagating along the X-axis will be introduced. The coordinates and components of velocity and pressure in both frames are shown as follows:

$$\left.\begin{array}{l} \varkappa = \bar{\varkappa} - c\acute{t}, \Upsilon = \bar{\Upsilon}, \widetilde{u}\left(\varkappa, \Upsilon\right) = \widetilde{U}\left(\bar{\varkappa}, \bar{\Upsilon}, \acute{t}\right) - c, \\ \widetilde{v}\left(\varkappa, \Upsilon\right) = \widetilde{V}\left(\bar{\varkappa}, \bar{\Upsilon}, \acute{t}\right), \widetilde{p}\left(\varkappa, \Upsilon\right) = \widetilde{P}\left(\bar{\varkappa}, \bar{\Upsilon}, \acute{t}\right) \end{array}\right\} \tag{14}$$

The continuity is satisfying and the Eqs. (8)–(10) become:

$$\begin{aligned} Re\delta\left[\left(\frac{\partial \Psi}{\partial y} + 1\right)\frac{\partial^2 \Psi}{\partial x \partial y} - \frac{\partial \Psi}{\partial x}\frac{\partial^2 \Psi}{\partial y^2}\right] = &- \frac{\partial p}{\partial x} + \delta\frac{\partial}{\partial x}\left(S_{xx}\right) + \frac{\partial}{\partial y}\left(S_{xy}\right) \\ &- \left(M^2 + \frac{1}{K}\right)\left(\frac{\partial \Psi}{\partial y} + 1\right) + \frac{Re}{Fr}\sin\alpha \end{aligned} \tag{15}$$

$$-Re\delta^3\left[\left(\frac{\partial \Psi}{\partial y} + 1\right)\frac{\partial^2 \Psi}{\partial x^2} + \frac{\partial \Psi}{\partial x}\frac{\partial^2 \Psi}{\partial x \partial y}\right] = - \frac{\partial p}{\partial y} + \delta^2\frac{\partial}{\partial x}\left(S_{xy}\right) + \delta\frac{\partial}{\partial y}\left(S_{yy}\right) + \frac{\delta^2}{K}\frac{\partial \Psi}{\partial x} - \delta\frac{Re}{Fr}\cos\alpha \tag{16}$$

$$Re\delta\left[\left(\frac{\partial \Psi}{\partial y} + 1\right)\frac{\partial \theta}{\partial x} - \frac{\partial \Psi}{\partial x}\frac{\partial \theta}{\partial y}\right] = \frac{1}{Pr}\left[\delta^2\frac{\partial^2 \theta}{\partial x^2} + \frac{\partial^2 \theta}{\partial y^2}\right] + Nt\left[\delta^2\left(\frac{\partial \theta}{\partial x}\right)^2 + \left(\frac{\partial \theta}{\partial y}\right)^2\right] \tag{17}$$

The dimensionless of stress components are:

$$\begin{aligned} & S_{xx}+\lambda_1\left\{\delta\left[\frac{\partial}{\partial t}+\left(\frac{\partial \Psi}{\partial y}+1\right)\frac{\partial}{\partial x}-\frac{\partial \Psi}{\partial x}\frac{\partial}{\partial y}\right]S_{xx}-2\delta S_{xx}\frac{\partial^2\Psi}{\partial x\partial y}-2S_{xy}\frac{\partial^2\Psi}{\partial y^2}\right\} \\ & +\frac{1}{2}\left(\lambda_1-\mu_1\right)\left[4\delta S_{xx}\frac{\partial^2\Psi}{\partial x\partial y}+2S_{xy}\left(\frac{\partial^2\Psi}{\partial y^2}-\delta^2\frac{\partial^2\Psi}{\partial x^2}\right)\right] \\ & =2\delta\frac{\partial^2\Psi}{\partial x\partial y} \end{aligned} \tag{18}$$

$$\begin{aligned} & S_{xy}+\lambda_1\left\{\delta\left[\frac{\partial}{\partial t}+\left(\frac{\partial \Psi}{\partial y}+1\right)\frac{\partial}{\partial x}-\frac{\partial \Psi}{\partial x}\frac{\partial}{\partial y}\right]S_{xy}+\delta^2 S_{xx}\frac{\partial^2\Psi}{\partial x^2}-S_{yy}\frac{\partial^2\Psi}{\partial y^2}\right\} \\ & +\frac{1}{2}\left(\lambda_1-\mu_1\right)\left(S_{xx}+S_{yy}\right)\left(\frac{\partial^2\Psi}{\partial y^2}-\delta^2\frac{\partial^2\Psi}{\partial x^2}\right) \\ & =\frac{\partial^2\Psi}{\partial y^2}-\delta^2\frac{\partial^2\Psi}{\partial x^2} \end{aligned} \tag{19}$$

$$\begin{aligned} & S_{yy}+\lambda_1\left\{\delta\left[\frac{\partial}{\partial t}+\left(\frac{\partial \Psi}{\partial y}+1\right)\frac{\partial}{\partial x}-\frac{\partial \Psi}{\partial x}\frac{\partial}{\partial y}\right]S_{yy}-2\delta^2 S_{xy}\frac{\partial^2\Psi}{\partial x^2}+2\delta S_{yy}\frac{\partial^2\Psi}{\partial x\partial y}\right\} \\ & +\frac{1}{2}\left(\lambda_1-\mu_1\right)\left[-4\delta S_{yy}\frac{\partial^2\Psi}{\partial x\partial y}+2S_{xy}\left(\frac{\partial^2\Psi}{\partial y^2}-\delta^2\frac{\partial^2\Psi}{\partial x\partial y}\right)\right] \\ & =-2\delta\frac{\partial^2\Psi}{\partial x\partial y} \end{aligned} \tag{20}$$

The expression for (11) and (12) is as follows:

$$\frac{\partial \Psi}{\partial y}=0, \theta=0 \; at \; y=\grave{h_1} \tag{21}$$

$$\frac{\partial \Psi}{\partial y}=0, \theta=1 \; at \;\; y=\grave{h_2} \tag{22}$$

Applying the large-wavelength approximation along with the small Reynolds number limit.

The following Eqs. (15)–(20) become:

$$\frac{\partial p}{\partial x}=\frac{\partial}{\partial y}\left(S_{xy}\right)-\left(M^2+\frac{1}{K}\right)\left(\frac{\partial \Psi}{\partial y}+1\right)+\frac{Re}{Fr}\sin\alpha \tag{23}$$

$$\frac{\partial p}{\partial y}=0 \tag{24}$$

$$\frac{\partial^2\theta}{\partial y^2}+Pr\;Nt\left(\frac{\partial \theta}{\partial y}\right)^2=0 \tag{25}$$

$$S_{xx}=\left(\lambda_1+\mu_1\right)S_{xy}\frac{\partial^2\Psi}{\partial y^2} \tag{26}$$

$$S_{xy}+\frac{1}{2}\left(\lambda_1-\mu_1\right)\left(S_{xx}+S_{yy}\right)\frac{\partial^2\Psi}{\partial y^2}-\lambda_1 S_{yy}\frac{\partial^2\Psi}{\partial y^2}=\frac{\partial^2\Psi}{\partial y^2} \tag{27}$$

$$S_{yy} = -\left(\lambda_1 - \mu_1\right) S_{xy} \frac{\partial^2 \Psi}{\partial y^2} \tag{28}$$

Equation (24) shows that p is not dependent on y, pressure can be eliminated from Eq. (23). Upon simplifying Eqs. (26)–(28), and introducing the pseudoplastic fluid parameter $\zeta = (\mu_1^2 - \lambda_1^2)$ We get the system:

$$\frac{\partial^2}{\partial y^2}\left(S_{xy}\right) - \left(M^2 + \frac{1}{K}\right) \frac{\partial^2 \Psi}{\partial y^2} = 0 \tag{29}$$

$$S_{xy} = \frac{\frac{\partial^2 \Psi}{\partial y^2}}{1 - \zeta \left(\frac{\partial^2 \Psi}{\partial y^2}\right)^2} \tag{30}$$

$$\frac{\partial^2 \theta}{\partial y^2} + Pr\ Nt \left(\frac{\partial \theta}{\partial y}\right)^2 = 0 \tag{31}$$

in accordance with the boundary constraints:

$$\Psi = -\frac{F}{2}, \frac{\partial \Psi}{\partial y} = 0, \theta = 0\ at\ y = \grave{h}_1 = -1 - m\left(x + t\right) - b \sin\left[2\pi x + \phi\right] \tag{32}$$

$$\Psi = \frac{F}{2}, \frac{\partial \Psi}{\partial y} = 0, \theta = 1\ at\ \ y = \grave{h}_2 = 1 + m\left(x + t\right) + a \sin\left[2\pi x\right] \tag{33}$$

in this context, $\zeta = (\mu_1^2 - \lambda_1^2)$ is defined as the pseudoplastic fluid parameter, while the symbol F is used to represent mean flows in a dimensionless form.

$$F\ \ (x, t) = Q + b \sin\left[2\pi x\right] + a \sin\left[2\pi x + \phi\right] \tag{34}$$

$$F = \int_{\grave{h}_1(x)}^{\grave{h}_2(x)} \frac{\partial \Psi}{\partial y}, Q \equiv \frac{\widetilde{q}}{cd}, dy = \Psi\left(\grave{h}_2\right) - \Psi\left(\grave{h}_1\right) \tag{35}$$

The amount of pressure rise per wavelength is given by the following equation:

$$\Delta p = \int_0^1 \frac{\partial p}{\partial x} dx \tag{36}$$

The lower wall's transfer heat coefficient can be found using this formula:

$$Z\left(x\right) = \frac{\partial \grave{h}_1}{\partial x} \left(\frac{\partial \theta}{\partial y}\right)_{y = \grave{h}_1} \tag{37}$$

Equations (29)–(31), together with the boundary constraints (32) and (33). The perturbation method was used in the numerical solution to obtain analytical equations for the heat transfer, temperature field, stream function, axial velocity, pressure distribution, pressure gradient, and nanoparticle concentration.

4. Solution Technique

Since the Eqs. (29)–(31) are not solvable by conventional methods to obtain exact solution, numerical approaches are adopted.In this context, the series solutions corresponding to small parameters are

derived using the perturbation technique. Specifically, the variables P, Ψ, F and Z are perturbed with respect to the fluid parameter ζ, while is perturbed with respect to the Prandtl number Pr. The series expansions are truncated and retained up to the first-order approximation.

$$\left.\begin{aligned} P &= P_0 + \zeta P_1 + \zeta^2 P_2 + \ldots, \\ \Psi &= \Psi_0 + \zeta \Psi_1 + \zeta^2 \Psi_2 + \ldots, \\ F &= F_0 + \zeta F_1 + \zeta^2 F_2 + \ldots, \\ Z &= Z_0 + \zeta Z_1 + \zeta^2 Z_2 + \ldots, \\ \theta &= \theta_0 + Pr\theta_1 + Pr^2\theta_2 + \ldots. \end{aligned}\right\} \tag{38}$$

4.1. **Zeroth-order equations.** The equations at this order are expressed as:

$$\frac{\partial^4 \Psi_0}{\partial y^4} - {N_1}^2 \frac{\partial^2 \Psi_0}{\partial y^2} = 0 \tag{39}$$

$$\frac{\partial p_0}{\partial x} = \frac{\partial^3 \Psi_0}{\partial y^3} - {N_1}^2 \left(\frac{\partial \Psi_0}{\partial y} + 1 \right) + \frac{Re}{Fr} \sin \alpha \tag{40}$$

$$\frac{\partial^2 \theta_0}{\partial y^2} = 0 \tag{41}$$

Where $({N_1}^2 = M^2 + \frac{1}{K})$ According to the boundary constraints listed below:

$$\Psi_0 = -\frac{F}{2}, \frac{\partial \Psi_0}{\partial y} = 0, \theta = 0 \;\; at \; y = \grave{h}_1 \tag{42}$$

$$\Psi_0 = \frac{F}{2}, \frac{\partial \Psi_0}{\partial y} = 0, \theta = 1 \;\; at \; y \; = \grave{h}_2 \tag{43}$$

zero class equations solutions are:

$$\Psi_0 = c_3 + y c_4 + \frac{e^{-yN_1} c_1 + e^{yN_1} c_2}{{N_1}^2}$$

$$\theta_0 = \frac{h_1 - y}{h_1 - h_2}$$

$$\frac{\partial P_0}{\partial x} = \frac{Re \;\; \sin[\alpha]}{Fr} + \left(\frac{-c_1 e^{-yN_1} {N_1}^3 + c_2 e^{yN_1} N_1^3}{N_1^2} \right) - \; N_1^2 \left(1 + c_4 + \frac{-c_1 e^{-yN_1} N_1 + c_2 e^{yN_1} N_1}{N_1^2} \right)$$

$$Z_0 = \frac{\partial h_1}{\partial x} \left(\frac{\partial \theta_0}{\partial y} \right)_{y = h_1} = - \frac{-\acute{m} - 2b\pi \cos[2\pi x + \vartheta]}{-2 - 2\acute{m}(t + x) - a \sin[2\pi x] - b \sin[2\pi x + \vartheta]}$$

4.2. **First-order equations.** The equations at this order are expressed as:

$$\frac{\partial^4 \Psi_1}{\partial y^4} + 3 \frac{\partial^4 \Psi_0}{\partial y^4} \left(\frac{\partial^2 \Psi_0}{\partial y^2} \right)^2 + 6 \left(\frac{\partial^3 \Psi_0}{\partial y^3} \right)^2 \left(\frac{\partial^2 \Psi_0}{\partial y^2} \right) - {N_1}^2 \frac{\partial^2 \Psi_1}{\partial y^2} = 0 \tag{44}$$

$$\frac{\partial p_1}{\partial x} - \frac{\partial^3 \Psi_1}{\partial y^3} - 3\frac{\partial^3 \Psi_0}{\partial y^3}\left(\frac{\partial^2 \Psi_0}{\partial y^2}\right)^2 + {N_1}^2 \frac{\partial \Psi_1}{\partial y} = 0 \tag{45}$$

$$\frac{\partial^2 \theta_1}{\partial y^2} + Nt\left(\frac{\partial \theta_0}{\partial y}\right)^2 = 0 \tag{46}$$

In accordance with the boundary constraints:

$$\Psi_1 = -\frac{F}{2}\frac{\partial \Psi_1}{\partial y} = 0, \theta = 0 \ \ at\ y = \grave{h}_1 \tag{47}$$

$$\Psi_1 = \frac{F}{2}, \frac{\partial \Psi_1}{\partial y} = 0, \theta = 1\ at\ y = \grave{h}_2 \tag{48}$$

First class equations solutions are:

$$\begin{aligned}\Psi_1 = c_7 + yc_8 + \frac{1}{8N_1}\Bigg(&- 2e^{-yN_1}\left(-6{c_1}^2 c_2 y - \frac{15{c_1}^2 c_2 + 4c_5}{N_1}\right) \\ &+ 2e^{yN_1}\left(-6c_1{c_2}^2 y + \frac{15c_1{c_2}^2 + 4c6}{N_1}\right) - \frac{{c_1}^3 e^{-3yN_1}}{N_1} - \frac{{c_2}^3 e^{3yN_1}}{N_1}\Bigg)\end{aligned}$$

$$\theta_1 = \frac{-\grave{h}_1\grave{h}_2 N_t - y\left(-\grave{h}_1 N_t - \grave{h}_2 N_t\right) - y^2 N_t}{2\left(\grave{h}_1 - \grave{h}_2\right)^2}$$

$$\begin{aligned}\frac{dp_1}{dx} = &- \frac{3\left(c_1 e^{-yN_1}N_1^2 + c_2 e^{yN_1}N_1^2\right)^2\left(-c_1 e^{-yN_1}N_1^3 + c_2 e^{yN_1}N_1^3\right)}{N_1^6} \\ &+ \frac{1}{8N_1}\Bigg(27{c_1}^3 e^{-3yN_1}N_1^2 + 36{c_1}^2 c2 e^{-yN_1}N_1^2 - 36c_1{c_2}^2 e^{yN_1}N_1^2 - 27{c_2}^3 e^{3yN_1}N_1^2 \\ &+ 2e^{-yN_1}\left(-6{c_1}^2 c_2 y - \frac{15{c_1}^2 c_2 + 4c_5}{N_1}\right)N_1^3 \\ &+ 2e^{yN_1}\left(-6c_1{c_2}^2 y + \frac{15c_1{c_2}^2 + 4c_6}{N_1}\right)N_1^3\Bigg) \\ &+ N_1^2(c8 + \frac{3{c_1}^3 e^{-3yN_1} + 12{c_1}^2 c_2 e^{-yN_1} - 12c_1{c_2}^2 e^{yN_1} - 3{c_2}^3 e^{3yN_1})}{8N_1} \\ &+ \frac{+2e^{-yN_1}\left(-6{c_1}^2 c_2 y - \frac{15{c_1}^2 c_2 + 4c_5}{N_1}\right)N_1}{8N_1} + \frac{2e^{yN_1}(-6c_1{c_2}^2 y + \frac{15c_1{c_2}^2 + 4c_6}{N_1})N_1}{8N_1})\end{aligned}$$

$$\begin{aligned}Z_1 &= \frac{\partial h_1}{\partial x}\left(\frac{\partial \theta_1}{\partial y}\right)_{y=h_1} \\ &= (-m - 2b\pi\cos\left[2\pi x + \vartheta\right]) \\ &\Bigg(-\frac{\left(-1 - m\left(t + x\right) - b\sin\left[2\pi x + \vartheta\right]\right)N_t}{\left(-2 - 2m\left(t + x\right) - a\sin\left[2\pi x\right] - b\sin\left[2\pi x + \vartheta\right]\right)^2} \\ &- \frac{-((1 + m(t + x) + a\sin\left[2\pi x\right])N_t)}{2\left(-2 - 2m\left(t + x\right) - a\sin\left[2\pi x\right] - b\sin\left[2\pi x + \vartheta\right]\right)^2}\end{aligned}$$

$$+\frac{(1+m(t+x)+b\sin[2\pi x+\vartheta])N_t}{2(-2-2m(t+x)-a\sin[2\pi x]-b\sin[2\pi x+\vartheta])^2}\Bigg)$$

5. Results and Discussion

This section examines the impact of the physical variables on flow characteristics, which is reviewed using graphs and numerical results. The trapping phenomenon, pressure gradient, pressure rise, and velocity distribution are all examined in the analysis. It is shown that these behaviors are affected by increasing the values of parameters such as the upper wall capacity coefficient (b), the phase difference coefficient (ϕ), the dimensionless flow rate (Q), and the lower wall capacity coefficient (a).

5.1. **Velocity profile.** Initially, Figs. 2-5 clearly show that the velocity distribution takes the form of a parabola., as shown in the graphs. These figures were plotted to investigate the influence of the Hartmann number M, the permeability parameter κ, the phase difference coefficient ϕ, and the average flow rate on velocity distribution Q. The value of $x = 2.001$ and $t = 2.001$ in all Figures. Fig 2 shows the effect of the Hartmann number (M) on velocity. The results show a decline in velocity at the center channel, whereas an inverse trend is observed near the boundaries. This is attributed to influence of the applied magnetic field, which impedes fluid movement and acts as an axial damping force that reduces the flow velocity. The opposite is true as the permeability parameter k rises, show Fig 4. Fig 5 illustrates the velocity increase progressively with the rise flow rate Q. Finally, Fig 3 illustrates how the phase difference coefficient affects the channel's velocity profile.

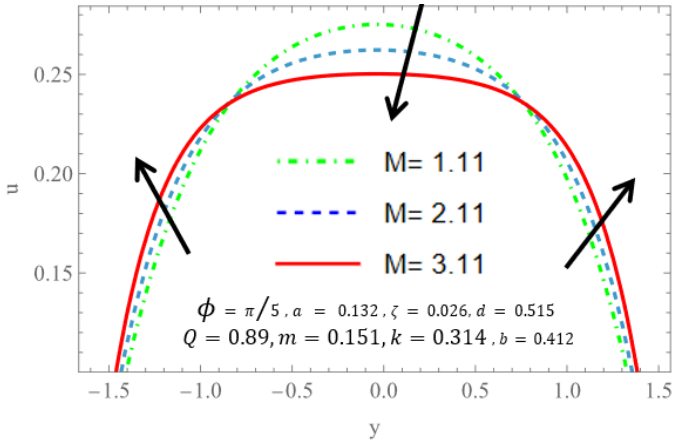

Figure 2. Presents the impact of different values to (M) on the velocity profile.

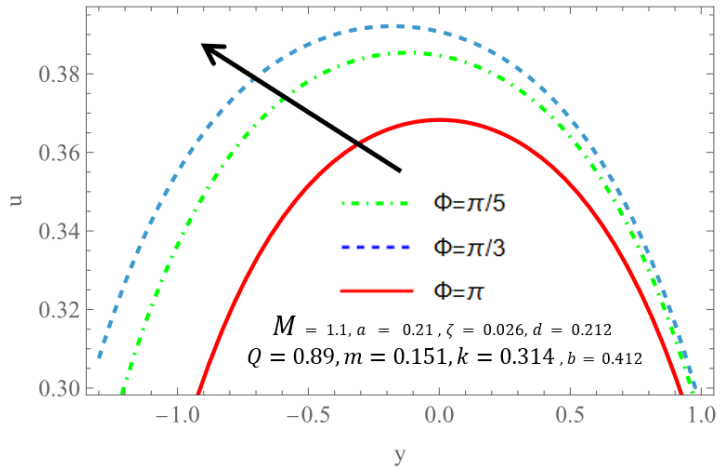

FIGURE 3. Presents the impact of different values to (ϕ) on the velocity profile.

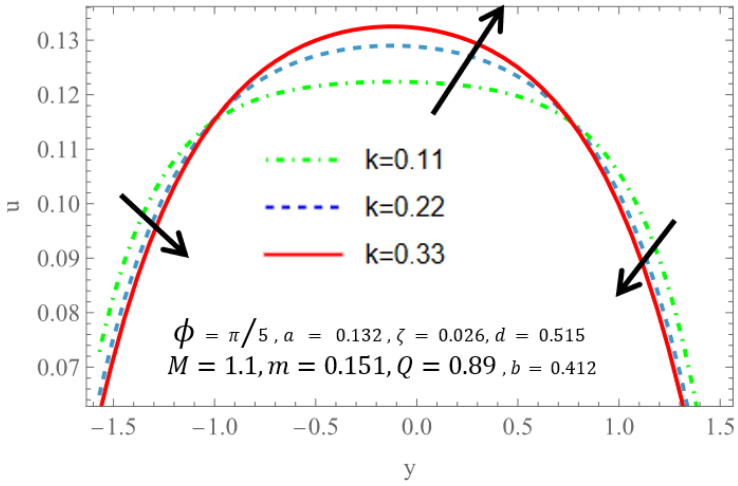

FIGURE 4. Presents the impact of different values to (k) on the velocity profile.

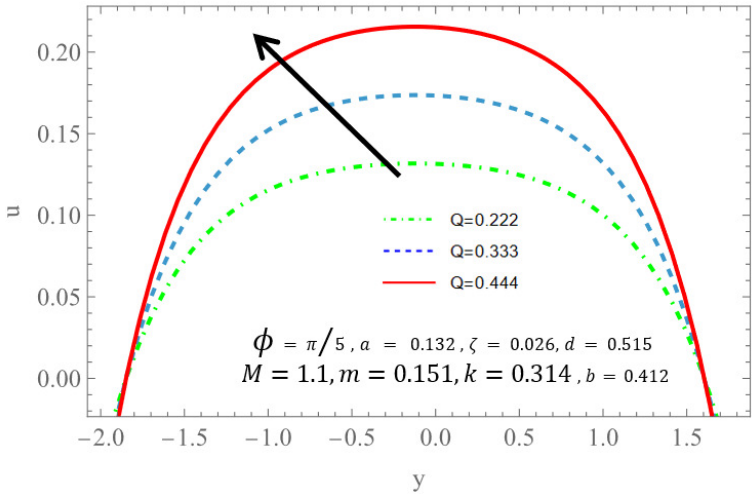

FIGURE 5. Presents the impact of different values to (Q) on the velocity profile.

5.2. **Temperature profile.** This part deals with the analysis of the effect of Prandtl number Pr, phase difference ϕ, non-uniform parameter m, and thermophoresis parameter Nt on temperature profile. These figures show that the temperature profiles are almost parabolic, with an increase in temperature observed in the center of the channel. Figures 6 and 7 shows that as Nt and Pr increase, the temperature rises. The impact of raising the non-uniformity parameter m on the channel's temperature distribution is shown in Figure 8. The findings show that higher values of m cause the temperature to rise in the channel's lower region while having the opposite effect in its upper region, where it progressively drops. In Figure 9, the complete opposite occurs.

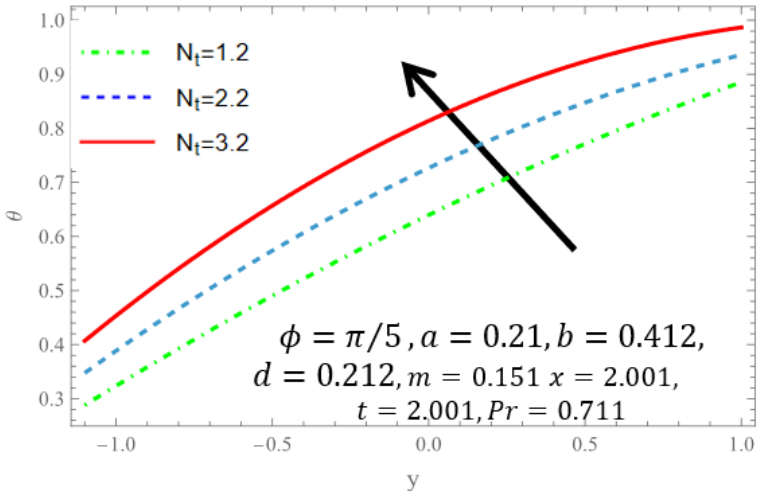

FIGURE 6. Presents the impact of different values to (Nt) on the temperature profile.

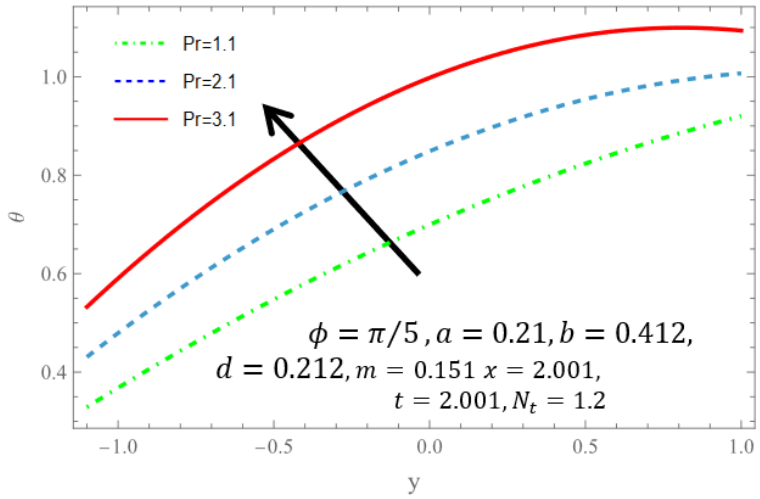

FIGURE 7. Presents the impact of different values to (Pr) on the temperature profile.

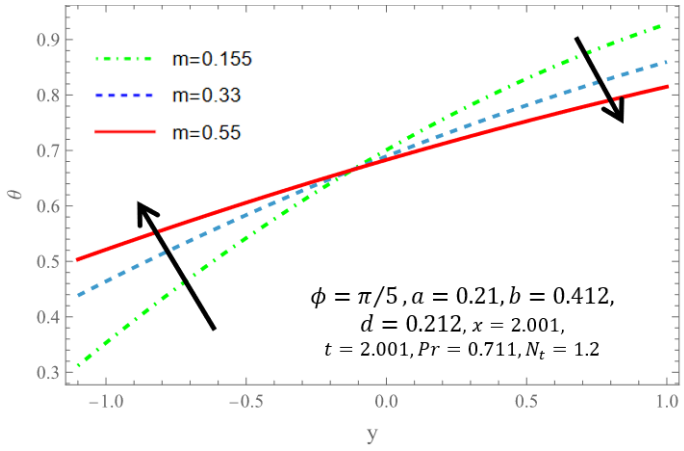

FIGURE 8. Presents the impact of different values to (m) on the temperature profile.

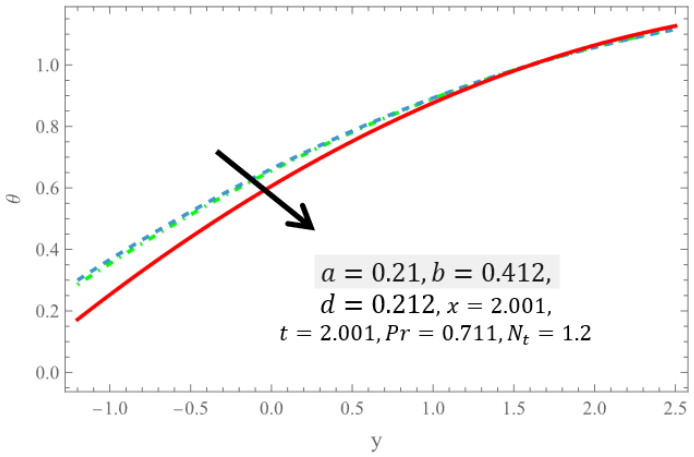

FIGURE 9. Presents the impact of different values to (ϕ) on the temperature profile.

5.3. **Pumping characteristics.** Figures 10, 11, 12 and 13 show how different physical parameters affect the average pressure increase. (Δp) as a function of the volumetric flow rate (Q). In all cases, Δp Lorentz force, which creates an additional opposing effect on the flow, weakening the pumping process.

Figure 12 shows the effect of the Reynolds number Re. Higher Re leads to a lower value of Δp at a constant flow rate. Physically, higher values of Re indicate a predominance of inertial effects over viscous forces, reducing pressure losses and resulting in a lower pumping pressure requirement. Finally, Figure 13 illustrates the effect of wave number α. Increasing α results in a lower Δp at the same flow rate. This is explained by the fact that increased wall undulation increases the frictional resistance within the channel, increasing pressure losses. Overall, the results indicate that pumping efficiency is significantly influenced by permeability coefficients and magnetic field, while both the Reynolds number and wave number also play important roles in controlling the amount of pressure increase within the channel.

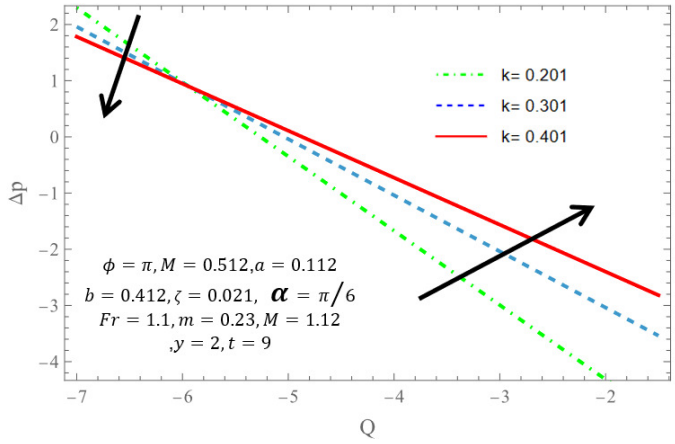

FIGURE 10. Presents the impact of different values to (k) on the average pressure rise.

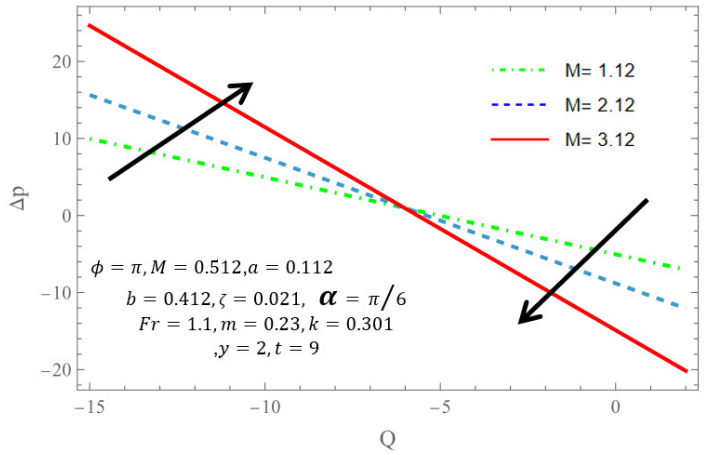

FIGURE 11. Presents the impact of different values to (M) on the average pressure rise.

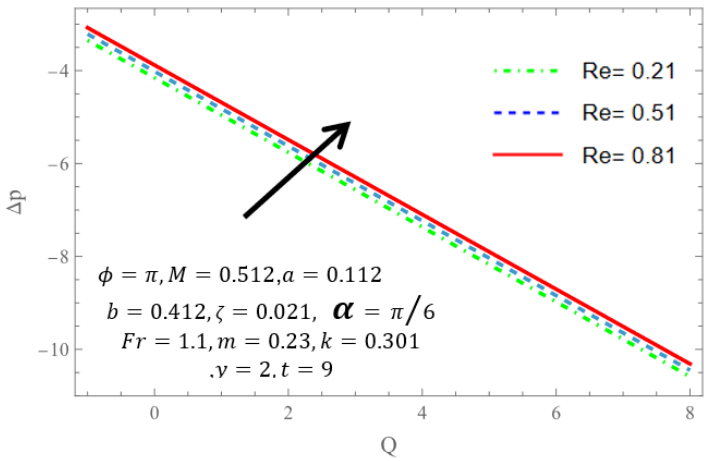

FIGURE 12. Presents the impact of different values to (Re) on the average pressure rise.

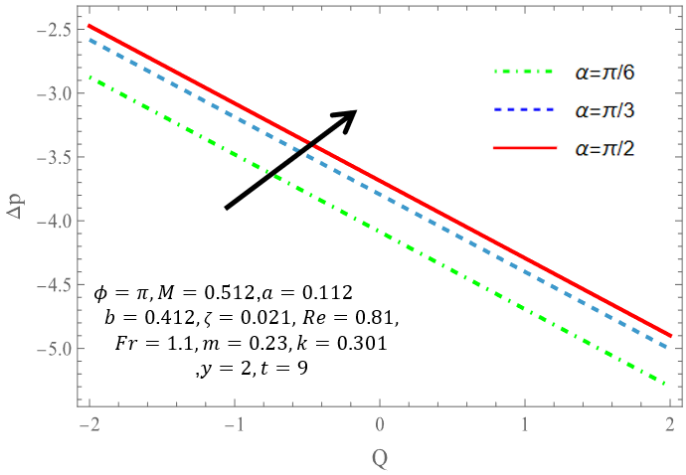

FIGURE 13. Presents the impact of different values to (α) on the average pressure rise.

5.4. **Heat transfer coefficient.** Figures 14, 15, 16 and 17 reflect the impact of peristalsis on the channel's upper wall heat transfer coefficient he results show that this coefficient varies as a result of sine waves propagating along the walls. Additionally, Figure 14 illustrates how the heat transfer coefficient increases as the value of M increases, while Figures 15, 16 and 17 show that the coefficient decreases as the values of Q, k, and ζ increase.

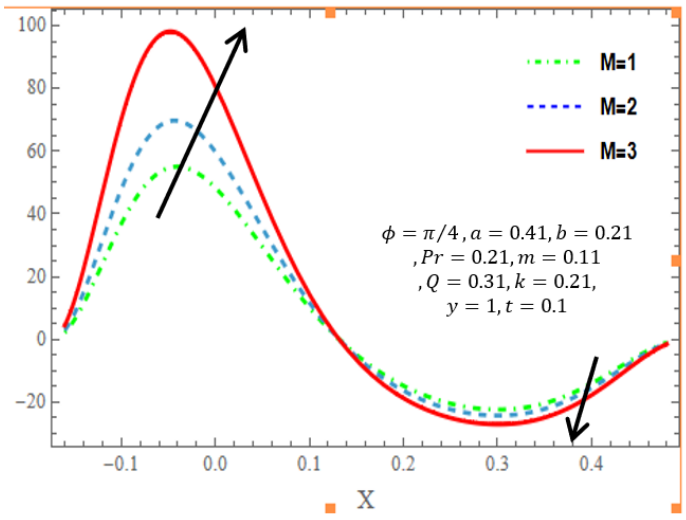

FIGURE 14. Presents the impact of different values to (M) on the heat transfer coefficient.

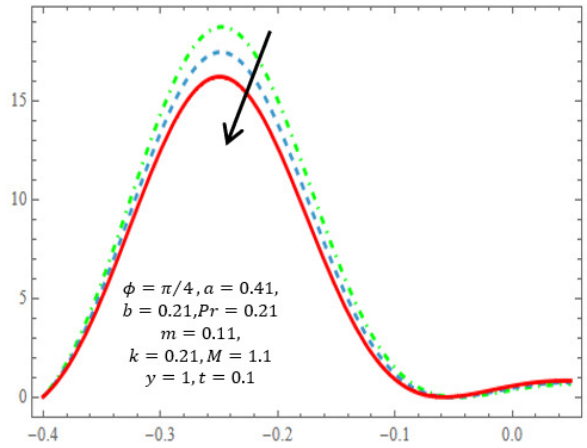

FIGURE 15. Presents the impact of different values to (Q) on the heat transfer coefficient.

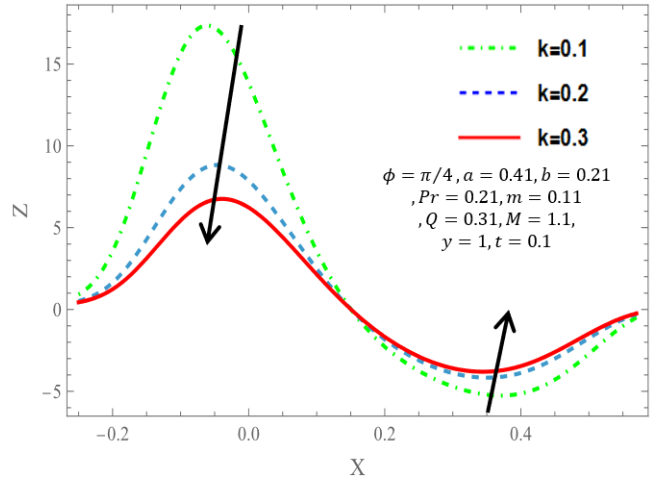

FIGURE 16. Presents the impact of different values to (k) on the heat transfer coefficient.

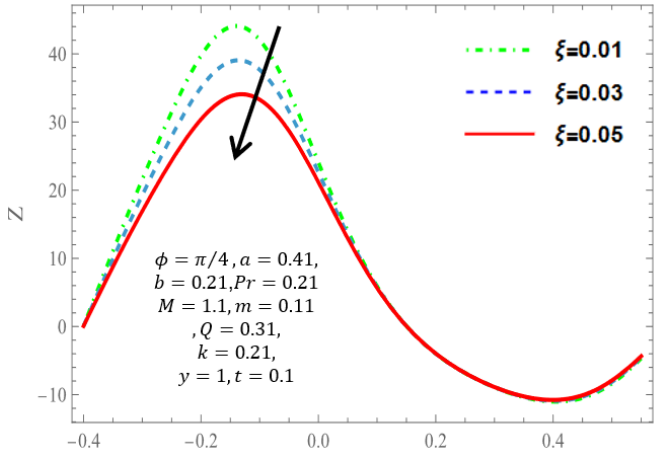

FIGURE 17. Presents the impact of different values to (ζ) on the heat transfer coefficient.

5.5. **Nusselt number.** Figures 18, 19 and 20 illustrate impact the variables to Nusselt number. Figures indicate that it rises (heat transfer improves) with rise values for m and falls in the channel's middle. increases at end the channel with increasing values of Pr and Nt.

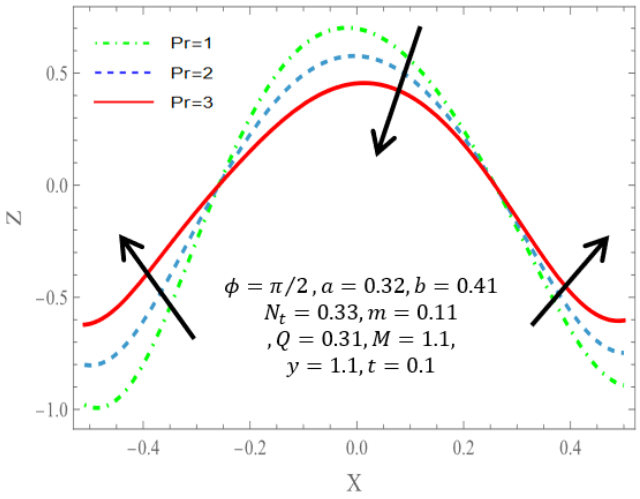

FIGURE 18. Presents the impact of different values to (Pr) on the Nusselt number.

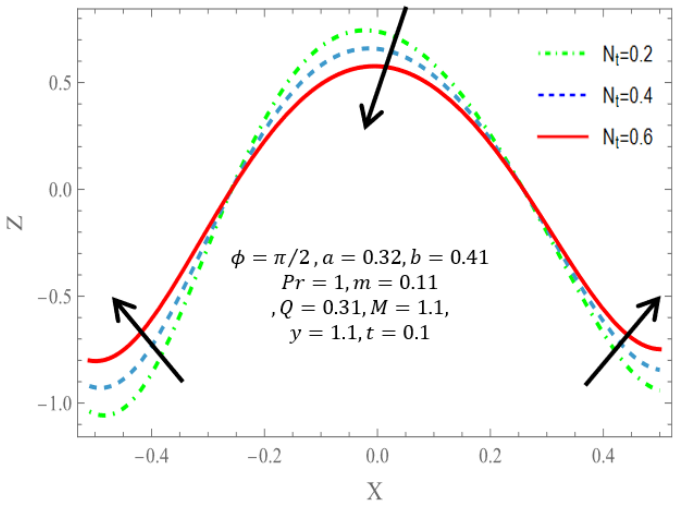

FIGURE 19. Presents the impact of different values to (Nt) on the Nusselt number.

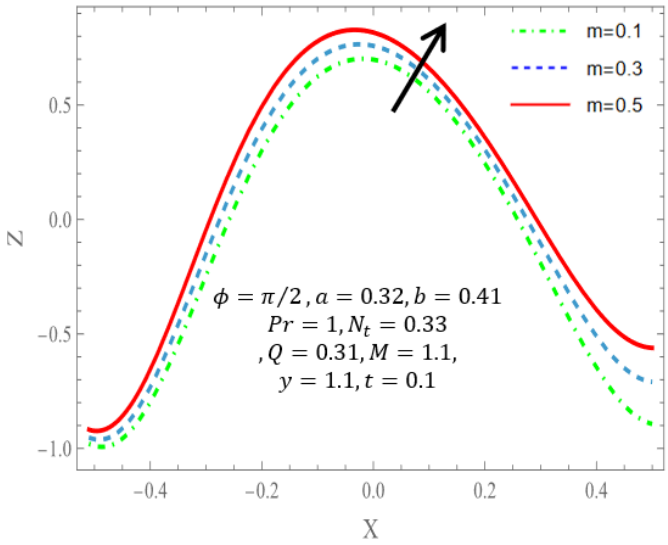

FIGURE 20. Presents the impact of different values to (m) on the Nusselt number.

5.6. **Trapping.** The trapping phenomenon corresponding to various values of m, Hartman number M, phase difference varying ϕ, and mean flow rate Q is depicted in Figures 21-24. It has been noted that as Q and M increase, so does the size of the trapped bolus. Additionally, it is noted that as m and ϕ increase, the trapped mass's volume decreases.

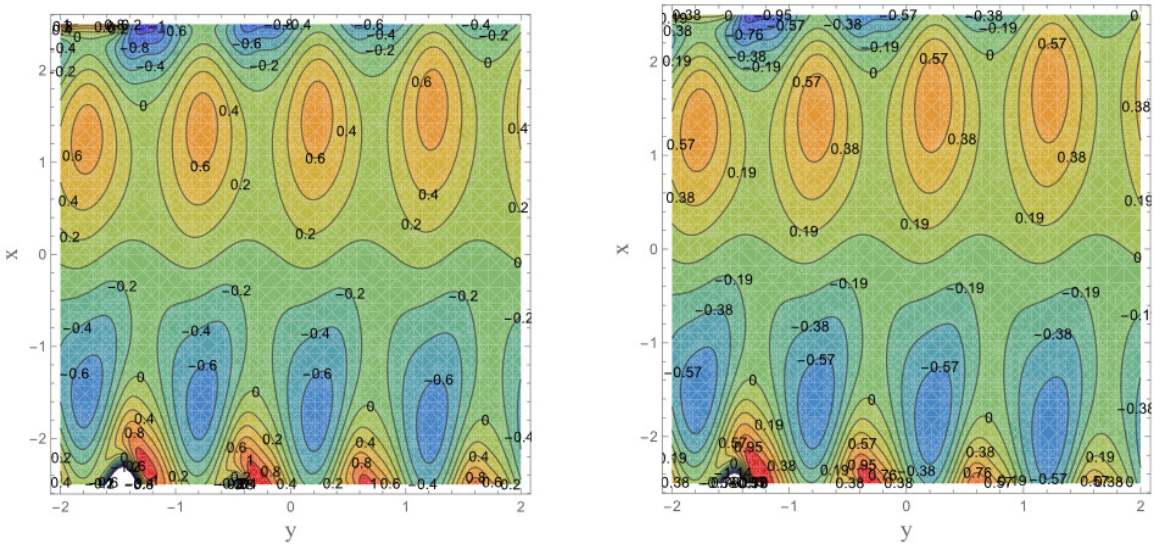

(A) $m = 0.113$ (B) $m = 0.141$

FIGURE 21. Stream lines for $a = 0.15, b = 0.43, \zeta = 0.026, d = 0.51, k = 0.31, Q = 0.83, M = 2.0, t = 3, m = 0.155, \phi = \pi/6, M = 0.6$.

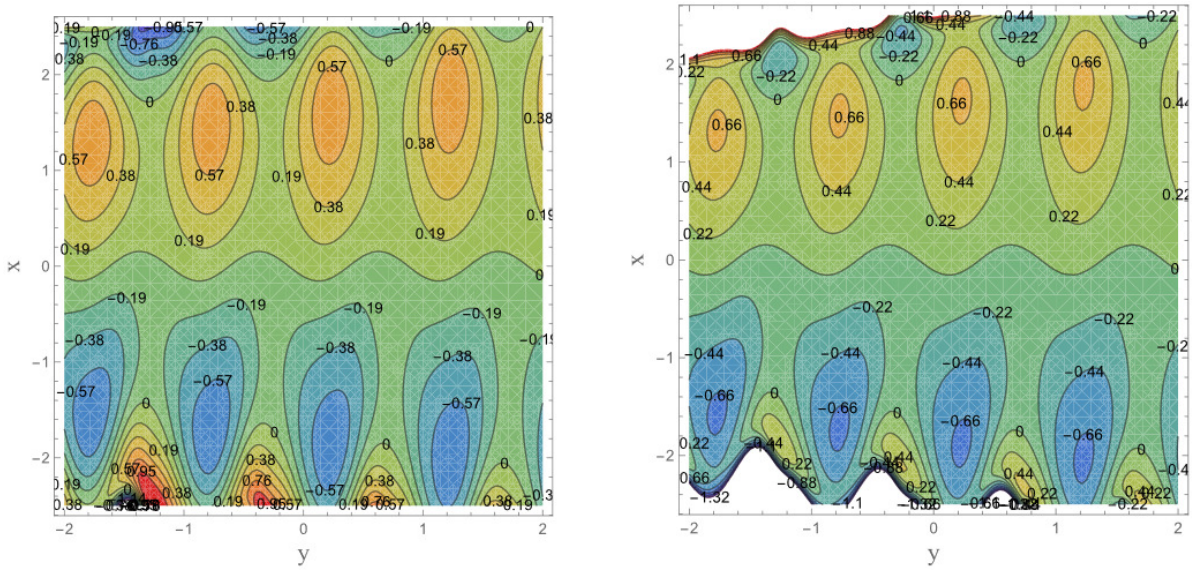

(A) $M = 0.6$ (B) $M = 2.2$

FIGURE 22. Stream lines for $a = 0.15, b = 0.43, \zeta = 0.026, d = 0.51, k = 0.31, Q = 0.83, M = 2.0, t = 3, m = 0.155, \phi = \pi/6$.

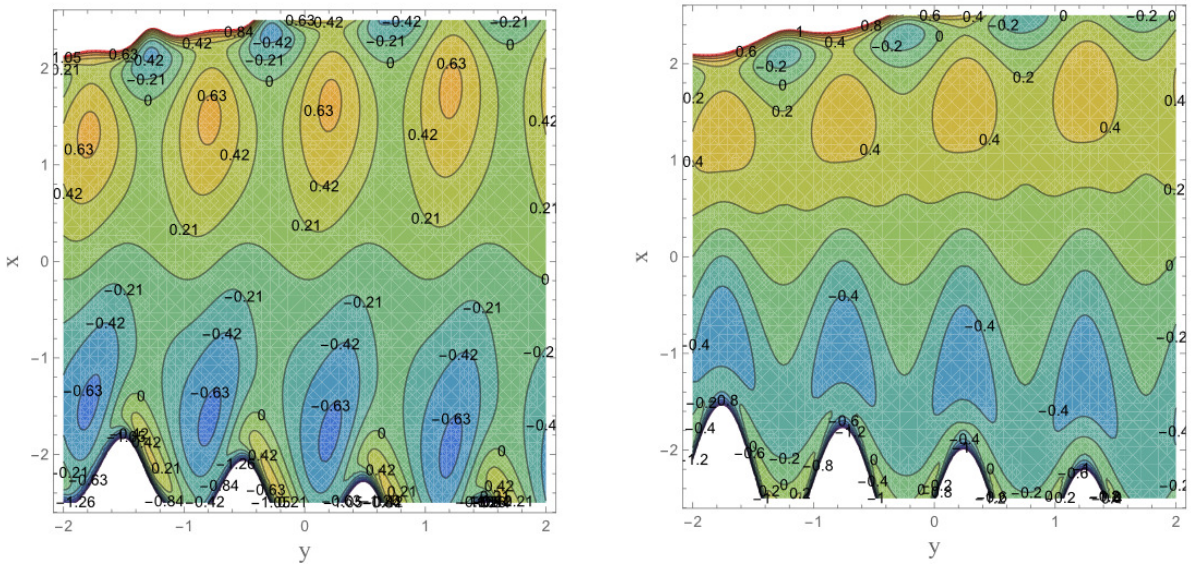

(A) $\phi = \pi/3.0$ (B) $\vartheta = \pi/1$

FIGURE 23. Stream lines for $a = 0.15, b = 0.43, \zeta = 0.026, d = 0.51, k = 0.31, Q = 0.83, M = 2.0, t = 3, m = 0.155$.

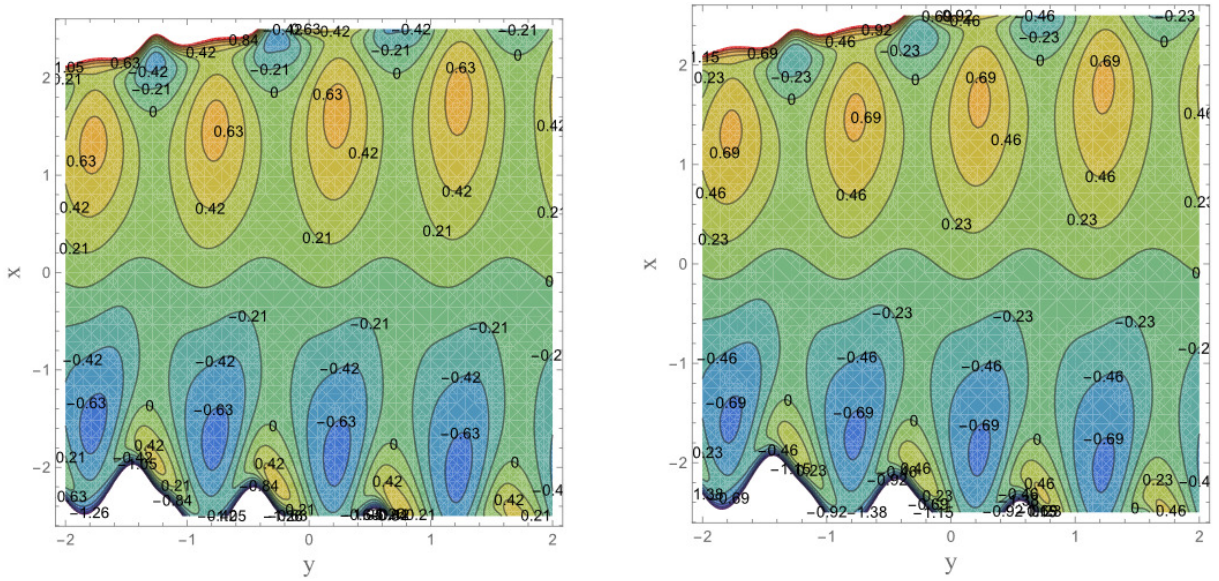

(A) $Q = 0.83$ (B) $Q = 0.9$

FIGURE 24. Stream lines for $a = 0.15, \phi = \pi/6, b = 0.43, \zeta = 0.026, d = 0.51, k = 0.31, Q = 0.83, M = 2.0, t = 3, m = 0.155$.

6. CONCLUSIONS

The findings demonstrated that raising the Hartmann number causes the flow velocity to drop, the average pressure to drop, the pumping process to weaken, the heat transfer coefficient to rise, and the trapped bolus to enlarge. This is because of the Lorentz force. As the permeability coefficient rises, the flow velocity increases, the necessary pumping pressure decreases, and the heat transfer coefficient decreases. Increase the phase difference coefficient leads to a decrease in the flow velocity, the temperature gradually decreases, and the volume of the trapped mass decreases. raise the parameter for thermophoresis It causes the temperature to rise and raises the Nusselt number at the end of the channel. A higher flow rate (Q) results in a larger trapped bolus, a decrease in the heat transfer coefficient, and an increase in velocity.

In the future, this analysis can be expanded to include additional physical effects such as rotation and chemical interactions. By examining the effects of varying viscosity, heat generation or absorption, and nanoparticle aggregation, practical medical and industrial applications will be better understood.

Nomenclature

Nomenclature			
ρ_p	Density of nano-particles	g	Acceleration
$\acute{\sigma}$	Fluid electrical Conductivity	Re	Reynolds number
D_T	Thermophoretic diffusion coefficient	Pr	Prandtl number
K_0	Permeability parameter	t	Time
ρ_f	Density of fluid	K	Darcy number
κ	Thermal conductivity of fluid	α	Inclination of the channel with the horizontal
λ	Wavelength	$\tilde{P}$	Dimensional Pressure
Q	Dimensionless mean flows	p	Dimensionless pressure
$\tilde{T}$	Fluid temperature	θ	Dimensionless temperature
B_0	Magnetic parameter	T_m	Fluid mean temperature
M	Hartman number	μ	Fluid viscosity
δ	Wavenumber	Nt	Thermophoresis parameter
h	Height of the channel	u	Velocity component in the x-direction
v	Velocity component in the y- direction	m	Non-uniform paremeter
b	Wave amplitude of walls		

Authors' Contributions. The manuscript's final draft has been read and approved by all authors. Each author made an equal contribution to this work.

Conflicts of Interest. The authors declare that there are no conflicts of interest regarding the publication of this paper.

References

[1] F. Abbasi, T. Hayat, A. Alsaedi, Numerical Analysis for MHD Peristaltic Transport of Carreau–Yasuda Fluid in a Curved Channel with Hall Effects, J. Magn. Magn. Mater. 382 (2015), 104–110. https://doi.org/10.1016/j.jmmm.2015.01.040.

[2] H.A. Ali, M. R. Salman, Influence of Rotation on Peristaltic Flow for Pseudoplastic Fluid: A Wavy Channel, Int. J. Optim. Control.: Theor. Appl. (IJOCTA) 14 (2024), 336–345. https://doi.org/10.11121/ijocta.1521.

[3] S.U.S. Choi, Enhancing Thermal Conductivity of Fluids With Nanoparticles, in: ASME International Mechanical Engineering Congress and Exposition, Vol. 17421, American Society of Mechanical Engineers, San Francisco, CA, USA, pp. 99–105, 1995. https://doi.org/10.1115/IMECE1995-0926.

[4] A. Ebaid, E.H. Aly, Exact Analytical Solution of the Peristaltic Nanofluids Flow in an Asymmetric Channel with Flexible Walls and Slip Condition: Application to the Cancer Treatment, Comput. Math. Methods Med. 2013 (2013), 825376. https://doi.org/10.1155/2013/825376.

[5] R. Ellahi, A. Riaz, S. Nadeem, Three Dimensional Peristaltic Flow of Williamson Fluid in a Rectangular Duct, Indian J. Phys. 87 (2013), 1275–1281. https://doi.org/10.1007/s12648-013-0340-2.

[6] O. Eytan, A.J. Jaffa, J. Har-Toov, E. Dalach, D. Elad, Dynamics of the Intrauterine Fluid–Wall Interface, Ann. Biomed. Eng. 27 (1999), 372–379. https://doi.org/10.1114/1.181.

[7] T. Hayat, F.M. Abbasi, A. Alsaedi, F. Alsaadi, Hall and Ohmic Heating Effects on the Peristaltic Transport of a Carreau–Yasuda Fluid in an Asymmetric Channel, Z. Naturforschung 69 (2014), 43–51. https://doi.org/10.5560/zna.2013-0074.

[8] T. Hayat, M. Shafique, A. Tanveer, A. Alsaedi, Hall and Ion Slip Effects on Peristaltic Flow of Jeffrey Nanofluid with Joule Heating, J. Magn. Magn. Mater. 407 (2016), 51–59. https://doi.org/10.1016/j.jmmm.2016.01.037.

[9] T. Hayat, H. Yasmin, S. Asghar, A.A. Hendi, Slip Effects on Peristaltic Transport in an Inclined Channel with Mass Transfer and Chemical Reaction, Appl. Bionics Biomech. 10 (2013), 41–58. https://doi.org/10.1155/2013/180646.

[10] S. Hina, M. Mustafa, T. Hayat, N.D. Alotaibi, On Peristaltic Motion of Pseudoplastic Fluid in a Curved Channel with Heat/mass Transfer and Wall Properties, Appl. Math. Comput. 263 (2015), 378–391. https://doi.org/10.1016/j.amc.2015.04.068.

[11] M. Kothandapani, J. Prakash, Effects of Thermal Radiation and Chemical Reactions on Peristaltic Flow of a Newtonian Nanofluid Under Inclined Magnetic Field in a Generalized Vertical Channel Using Homotopy Perturbation Method, Asia-Pac. J. Chem. Eng. 10 (2015), 259–272. https://doi.org/10.1002/apj.1870.

[12] T.W. Latham, Fluid Motions in a Peristaltic Pump, Ph.D. Thesis, Massachusetts Institute of Technology, 1966.

[13] S. Maiti, J. Misra, Peristaltic Flow of a Fluid in a Porous Channel: A Study Having Relevance to Flow of Bile Within Ducts in a Pathological State, Int. J. Eng. Sci. 49 (2011), 950–966. https://doi.org/10.1016/j.ijengsci.2011.05.006.

[14] K.S. Mekheimer, Y. Abd elmaboud, A.I. Abdellateef, Peristaltic Transport Through Eccentric Cylinders: Mathematical Model, Appl. Bionics Biomech. 10 (2013), 19–27. https://doi.org/10.1155/2013/902097.

[15] K. Ramesh, M. Devakar, Magnetohydrodynamic Peristaltic Transport of Couple Stress Fluid Through Porous Medium in an Inclined Asymmetric Channel with Heat Transfer, J. Magn. Magn. Mater. 394 (2015), 335–348. https://doi.org/10.1016/j.jmmm.2015.06.052.

[16] M.R. Salman, A.M. Abdulhad, Soret and Dufour Effects in MHD Peristalsis of Pseudoplasticnano Fluid with Porous Medium in Tapered Channel, Int. J. Sci. Res. 6 (2017), 1939–1951. https://doi.org/10.21275/art20179072.

[17] M. R. Salman, A. M. Abdulhadi, Analysis of Heat and Mass Transfer in a Tapered Asymmetric Channel during Peristaltic Transport of (Pseudoplastic Nanofluid) with Variable Viscosity Under the Effect of (MHD), J. Al-Qadisiyah Comput. Sci. Math. 10 (2018), 80–96. https://doi.org/10.29304/jqcm.2018.10.3.408.

[18] M.R. Salman, A.M. Abdulhadi, Effects of MHD on Peristalsis Transport and Heat Transfer With Variables Viscosity in Porous Medium, Int. J. Sci. Res. 7 (2018), 612–623.

[19] S. Shehzad, F. Abbasi, T. Hayat, F. Alsaadi, Model and Comparative Study for Peristaltic Transport of Water Based Nanofluids, J. Mol. Liq. 209 (2015), 723–728. https://doi.org/10.1016/j.molliq.2015.05.058.

[20] D. Tripathi, O.A. Bég, A Study on Peristaltic Flow of Nanofluids: Application in Drug Delivery Systems, Int. J. Heat Mass Transf. 70 (2014), 61–70. https://doi.org/10.1016/j.ijheatmasstransfer.2013.10.044.